Contents lists available at ScienceDirect

Cement and Concrete Research

A chemo-poromechanical model of oilwell cement carbonation under CO_2 geological storage conditions

A. Fabbri *, N. Jacquemet, D.M. Seyedi

BRGM, 3 avenue Claude Guillemin, 45060 Orléans Cedex 2, France

ARTICLE INFO

ABSTRACT

A poromechanical model is developed to identify how chemical reactions of carbonation may impact the mechanical behaviour of wellbore cement in the context of CO_2 storage. The model enables the evaluation of pore overpressure, porosity and solid-skeleton strain evolutions during the carbonation process. The major chemical reactions occurring within cement and their consequences on the volumes of dissolved cement matrix and precipitated carbonate are identified. This information is imported into a poromechanical model and the risk of damage is estimated through the calculation of the free energy stored within the solid matrix. A semi-analytical solution is proposed and applied to a simplified 1D cement carbonation example. The risk of damage of the cement structure submitted to intrusion of aqueous CO_2 is estimated. A set of parametric studies is carried out to investigate the effect of medium permeability and effective diffusion coefficient on the damage risk.

1. Introduction

The stabilization of the atmospheric CO_2 concentration requires CO_2 emissions to drop well below current levels. To reach this goal, several available strategies have been identified by Pacala and Socolow [1], including demand reduction, efficiency improvements, the use of renewable and nuclear power, and carbon capture and storage (CCS) [2]. This latter consists in capturing CO_2 at the emission spots and storing it in the subsurface where it will no longer contribute to global warming. Depleted oil and gas reservoirs, unmined coal seams, and particularly saline aquifers (deep underground porous reservoir rocks saturated with brackish water or brine), can be used for the storage of CO_2. At depths below about 800–1000m, CO_2 remains under supercritical state and has a liquid-like density and a gas-like viscosity that provide efficient utilization of underground storage space provided by the pores of sedimentary rocks [3,4].

Demonstration of the safety and integrity of CCS projects is a key factor for industrial deployment of this technology. Indeed, CO_2 injection may induce various geochemical, thermo-hydraulic and geomechanical phenomena in different spatial and temporal scales (e.g. [5–8]). The effects of these phenomena on the performance and integrity of the storage site must be studied. In a scenario based safety approach, natural and artificial discontinuities (i.e., faults and wells) are considered as potential leakage pathways. (e.g. [9]). Although the CO_2 injection well

should be cemented with a CO_2 resistant cement (commonly low-pH cement) [10], the CO_2 plume should encounter abandoned wells, which are rather cemented with conventional cements. The durability of cement used for existing oil and gas wells is thus of main interest for the safety assessment analysis of the CO_2 geological storage.

The carbonation of cement (reaction between carbonic acid and cement minerals) in CO_2 geological storage-relevant conditions (high pressure, high temperature, and geological fluids) provokes petrophysical (hydraulic conductivity and diffusivity) and mechanical changes. This effect was illustrated by laboratory experiments [11–15], field observations [16] and both decimetre- and field-scale reactive transport numerical simulations [17,18]. Moreover, in a recent study [19], a quantitative mechanical post-characterization of Portland cement based samples submitted to carbonation under deep downhole conditions (90 °C and 28 MPa) was performed. The results show a concentration of micro-cracks, i.e. potential pathways for CO_2 migration, at the interface between the carbonated and the un-carbonated zones of the sample. The chemical reactions during the carbonation process may thus engender enough mechanical stresses (in some particular conditions) on the cement solid matrix to damage it. Consequently, the sealing capacity could be altered, even though when the cement is properly placed and initially provides an effective hydraulic seal for the reservoir fluids. In this context, the development of a comprehensive quantitative assessment of the stress and strain fields of well cement during its carbonation process is necessary.

Commonly, the coupling between the geochemical processes and the mechanical behaviour is made through an external chaining of geochemical and mechanical codes [20]. This kind of coupling is particularly useful for large scale calculations but cannot provide

* Corresponding author. Tel.: +33 6 78 38 18 79.
 E-mail addresses: a.fabbri@brgm.fr (A. Fabbri), n.jacquemet@brgm.fr
(N. Jacquemet), d.seyedi@brgm.fr (D.M. Seyedi).

sufficient accuracy for local highly non-linear and/or time dependant chemo-mechanical simulations [21]. The goal of this paper is to present a coupling approach based on the framework of poromechanics. In this view, the major hydro-chemical processes that impact the macroscopic mechanical behaviour are directly included in the model. All the hydraulic, chemical and mechanical equations are then solved simultaneously.

Theoretical development of the poromechanical model is presented in sections two and three. In this framework the carbonate crystals have their own behaviour and can stress the surrounding matrix. Let us underline that in CCS context, the material will be affected by an acidic fluid during a long period (more than 1000 years), and thus, the stability of the carbonate crystal may not be insured. The proposed approach is particularly pertinent as it allows the study of either the mechanical state (damage, hardening/softening…) of the cement matrix alone or of the (cement and carbonate) system.

A semi-analytical solution of this problem is then used in order to evaluate the mechanical impact of the carbonation of a simplified 1D cement structure, initially submitted to homogeneous temperature, pressure and external stress. The major chemical reactions that produce a significant variation of porosity and/or pore overpressure within the porous network are identified. The characterized major reactions are then imported into the developed poromechanical model to quantify the pore overpressure evolution during the carbonation/dissolution process. The risk of damage is estimated through the calculation of the free energy stored within the solid matrix for a range of possible permeability and effective diffusivity of the porous medium.

Let us emphasise that the aim of the present study is not to predict the *in-situ* durability of existing well cement but to illustrate the capacities of the developed method to quantify the effect of the carbonation process on the mechanical behaviour. The choice of numerical model (1D) and values of different parameters must be seen in that way.

2. Thermodynamics of cement matrix carbonation

Let us consider that the carbonated cement is composed of a solid cement matrix (index M), which could be healthy or leached, and of calcium carbonate crystals (calcite, aragonite or vaterite) (index C). The cement matrix is made of the minerals referred as M_i. Finally, the in-pore fluid (index F) is composed by dissolved species (α) and a solvent (water molecule, w). The list of symbols used in the following is reported in Appendix A.

2.1. Skeleton and effective porosities

Let us note Ω_0 as the initial volume of cement Representative Elementary Volume (REV). The initial porous volume is $\phi_0 \Omega_0$, where ϕ_0 stands for the initial porosity. In order to scan the effect of carbonate precipitations on the porous solid behaviour, the effective porosity of the porous medium ϕ_F and the cement skeleton porosity ϕ need to be separated. The first one corresponds to the porous space filled by the in-pore fluid, and the second is the volume of the non-cementitious phases (i.e. fluids + carbonates) per unit of porous medium volume. The relation between these porosities reads (Fig. 1):

$$\phi = \phi_F + \phi_C \tag{1}$$

where $\phi_C \Omega_0$ is the current volume of carbonate crystals.

Each porosity (ϕ_F and ϕ_C) can be changed due to deformation of the porous network, noted φ_i, $i =$ F or C (concept originally introduced by Olivier Coussy [22,23]), or due to chemical reactions. This partition of porosity is illustrated in Fig. 2.

The chemical contribution to porosity variations is caused by the cement matrix leaching, noted V_M, and by the carbonate precipitation,
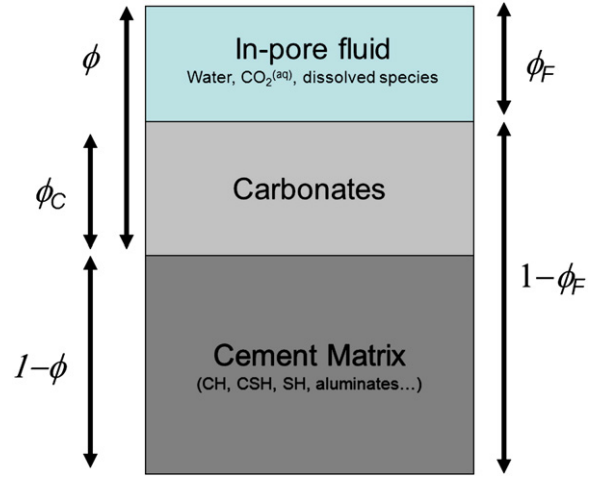

Fig. 1. Schematic representation of the porosities used in the model.

noted V_C. Cement leaching and carbonate precipitation can be linked to the molar quantity of cement and carbonate minerals through:

$$V_M = \sum_{M_i} \nu_{Mi} \left(n_{Mi,0} - n_{Mi} \right); V_C = \nu_C n_C \tag{2}$$

where n_j is the quantity of moles of $j = M_i, C$ per unit of porous medium volume and ν_j is the molar volume of j. The index 0 refers to the initial state. Evolutions of ϕ_F and ϕ_C can be expressed as:

$$\phi_F = \Phi S_F + \varphi_F; \quad \phi_C = \Phi S_C + \varphi_C \tag{3}$$

where S_F and $S_C = 1 - S_F$ are respectively the Lagrangian saturations of in-pore fluid and carbonate crystal that satisfy:

$$S_F = \frac{\Phi - V_C}{\Phi}; \; S_C = \frac{V_C}{\Phi}; \; \Phi = \phi_0 + V_M \tag{4}$$

In Eq. (4), $\Phi = (\phi_0 + V_M)$ stands for the porosity of the skeleton prior to any mechanical deformation.

2.2. In-pore fluid and carbonate crystal equilibrium

The carbonate precipitation can be written in the following form:

$$Ca^{2+} + CO_3^{2-} \rightarrow CaCO_3 \tag{5}$$

The thermodynamic equilibrium between the carbonate and the in-pore fluid is assumed to be reached at each time and within each representative elementary volume. Consequently, we get:

$$\mu_C = \mu_{Ca^{2+}} + \mu_{CO_3^{2-}} \tag{6}$$

where μ_C is the chemical potential of the carbonate crystal and $\mu_{Ca^{2+}} + \mu_{CO_3^{2-}}$ is the chemical potential of the dissolved crystal, composed of Ca^{2+} and CO_3^{2-}. Under these notations, and under isothermal conditions, Gibbs–Duhem equation applied separately to the solid crystal and the in-pore solution provides [22]:

$$\phi_C \frac{dp_C}{dt} = n_C \frac{d\mu_C}{dt} \tag{7}$$

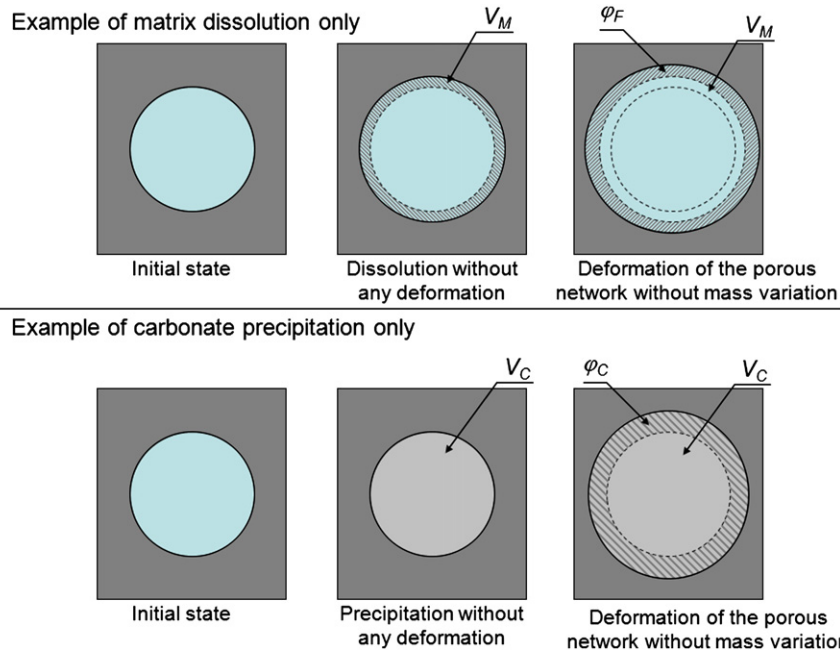$$\phi_F \frac{dp_F}{dt} = \sum_{i=\alpha,w} n_i \frac{d\mu_i}{dt} \tag{8}$$

Fig. 2. Schematic representation of the distinction between the chemical and mechanical contribution to the porosity variation. For the sake of simplicity, this figure assumes that pores are fully filled by either in-pore fluid or carbonate crystal, which will not be necessarily the case in a real system.

where p_F and p_C are the fluid and the crystal pressure respectively. They are linked through the mechanical equilibrium of the carbonate/fluid interface (Young–Laplace law):

$$p_C - p_F = \gamma_{FC} C_{FC} \qquad (9)$$

where γ_{FC} is the calcium carbonate/water interface energy, which can vary between 60 mN/m and 80 mN/m [24] and C_{FC} is the interface curvature. It is commonly assumed that the curvature of the crystal is bounded by the curvature of the porous space where it precipitates (e.g. [25]).

Several studies [14,26] investigated the evolution of the pore size distribution of an Ordinary Portland Cement during supercritical carbonation from mercury intrusion porosimetry (MIP) tests. These studies underline that the carbonate crystal will first precipitate within larger pores and then within smaller ones, leading to a progressive reduction of the global porosity. Then, for a given material, the radius of the pore where the carbonate crystal will precipitate, which is the threshold radius of an MIP test, can be estimated as a function of the global porosity (ϕ_F).

Let us consider a spherical crystal/fluid interface so that $C_{FC} = 2/R$, where R is the radius of the interface assumed to be close to the pore radius. Fluid/crystal pressure difference ($p_C - p_F$) evolution with effective porosity (ϕ_F) reads:

$$p_C - p_F = \frac{2\gamma_{FC}}{R_{th}(\phi_F)} \qquad (10)$$

where $R_{th}(\phi_F)$ is the radius of the largest pore available for the carbonated porous medium with a porosity equal to ϕ_F. This relationship will be different for each tested material. In the particular case of a class G cement cured at 80 °C, a threshold radius of 150 nm for a non-carbonated specimen ($\phi_F = 33\%$) can be considered [14]. The threshold radius is reduced to 15 nm after a half day of carbonation ($\phi_F = 23\%$) and close to 5 nm after 3 weeks of carbonation ($\phi_F = 18\%$). The variation of $p_C - p_F$ with ϕ_F from MIP data reported by [14] is shown in Fig. 3.

2.3. In-pore fluid–cement matrix equilibrium

The cement minerals' dissolution/precipitation reactions can be written as:

$$M_i \rightarrow \sum_{j=\alpha,w} a_{j,M_i} j \qquad (11)$$

where M_i is the mineral that is dissolved or precipitates (e.g. $M_i = $ CH, C–S–H, SiO_2...), while a_{j,M_i} stands for the relative stoichiometric coefficient of the dissolved species ($j = \alpha$) (e.g. $\alpha = Ca^{2+}$, OH^-,...), or water molecules ($j = w$) involved in the reaction ($a_{j,M_i} < 0$ if $j = \alpha,w$ is a reactant and $a_{j,M_i} > 0$ if $j = \alpha,w$ is a product). In this case, the chemical equilibrium can be expressed by:

$$\mu_{M_i} - \sum_{j,M} a_{j,M_i} \mu_j = 0; \ j = \alpha, w \qquad (12)$$

where μ_{M_i} is the chemical potential of mineral M_i, while μ_j is the chemical potential of $j = \alpha,w$.
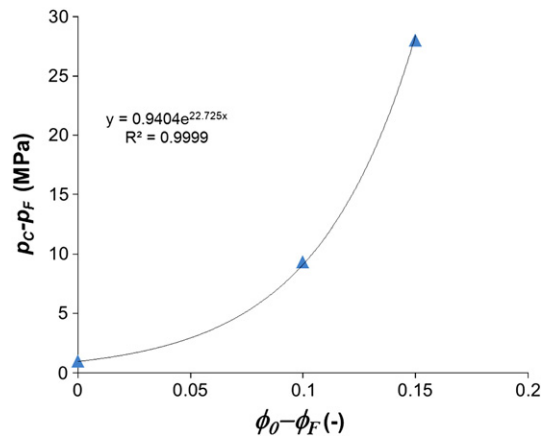

Fig. 3. Relation between the crystallization pressure and the overall porosity variation from [14] MIP data.

2.4. In-pore fluid mole balance

The change in the current molar quantity of species (dn_i/dt) is due to exchange of molecules with the adjacent infinitesimal elements or from the phase transformations occurring within the elementary porous space $d\Omega_0$. The continuity equations are then read:

$$\frac{dn_C}{dt} = \dot{n}_C; \frac{dn_{M_i}}{dt} = \dot{n}_{M_i}; \frac{dn_i}{dt} = -\underline{\nabla} \cdot \underline{\omega}_i + \dot{n}_i; i = \alpha, w \tag{13}$$

where $\dot{n}_{M_i}$, $\dot{n}_C$ and $\dot{n}_i$ are respectively the mole variation due to the chemical reactions of the cement mineral M_i, carbonates, and dissolved species. These mole variations can be linked through Eqs. (5) and (11) by the following relations:

$$\dot{n}_C = -\dot{n}_{Ca^{2+},C} = -\dot{n}_{CO_3^{2-},C} \text{ for carbonate precipitations} \tag{14}$$

$$\dot{n}_{M_i} = -\frac{\dot{n}_{i,M_i}}{a_{i,M_i}}, i = \alpha, w \text{ for matrix mineral leaching} \tag{15}$$

where $\dot{n}_{i,J}$ refers to the mole variation of phase $i = \alpha, w$ due to the precipitation/dissolution of carbonates ($J = C$) or of the cement mineral M_i ($J = M_i$).

Finally, $\underline{\omega}_i$, is the mole transport of phase $i = \alpha, w$. It is the combination of the diffusion/hydrodynamic dispersion of the molecule and its advective transport, thus:

$$\underline{\omega}_i = -d_{eff} \underline{\nabla} C_i - C_i \frac{\kappa}{\eta_F} \underline{\nabla} p_F \tag{16}$$

where $C_i = n_i / \phi_F$ is the molar concentration of phase i, p_F the fluid pressure, and η_F the dynamic viscosity of the fluid, while d_{eff} and κ are respectively the effective diffusivity/dispersivity coefficient (assumed to be the same for all species) and the intrinsic permeability.

3. Poromechanical modelling

3.1. Mechanical behaviour of in-pore water and carbonate crystal

For isothermal transformations, the density of the fluid phase satisfies [27]:

$$\frac{1}{\rho_F} \frac{d\rho_F}{dt} = \frac{1}{K_F} \frac{dp_F}{dt} + \sum_{i=\alpha,w} \gamma_i \frac{dn_i}{dt} \tag{17}$$

where K_F and p_F are the bulk modulus and the pressure of the in pore fluid respectively while $\gamma_i = \rho_F d(1/\rho_F)/dn_i|_{p_F,n_{j,j\neq i}}$ stands for the variation of the in-pore fluid density due to the variation of its composition. This density variation can be written as a function of the partial molar volume of phase i (i.e. $\bar{v}_i = d\phi_F/dn_i|_{p_F,n_{j,j\neq i}}$):

$$\gamma_i = \frac{\mathcal{M}_i}{m_F} - \frac{\bar{v}_i}{\phi_F} \tag{18}$$

where $\mathcal{M}_i$ is the molar mass of $i = \alpha, w$.

It can be reasonably assumed that the energy associated to the shear stress transmitted to the carbonate crystal–solid matrix interface during the crystal precipitation is negligible regarding the energy associated to the normal stress. Consequently, the carbonate crystal mechanical behaviour can be described by:

$$\frac{1}{\rho_C} \frac{d\rho_C}{dt} = \frac{1}{K_C} \frac{dp_C}{dt} \tag{19}$$

where K_C, ρ_C and p_C are the bulk modulus, density and pressure of the carbonate crystal ($j = C$) respectively.

3.2. Poroelastic state equations of the cement skeleton

The thermodynamic background used here is developed in detail in [22] and [28] and reported in Appendix B. The starting point of this approach is to combine the first and the second laws of thermodynamics applied to the whole porous medium:

$$([\sigma] - [\sigma_0]) : \frac{d[\varepsilon]}{dt} - \sum_{M_i} \left(v_{M_i}(p_a - p_0) - \mu_{M_i} \right) \dot{n}_{M_i} + \sum_{J=F,C} \left(p_J - p_0 \right) \frac{d\varphi_J}{dt} - \frac{dW}{dt} \geq 0 \tag{20}$$

where W is the free energy of the solid matrix, $[\sigma]$ and $[\varepsilon]$ are the stress and strain tensors, and p_a the average pore pressure, defined by:

$$p_a = S_F p_F + S_C p_C \tag{21}$$

Finally, $[\sigma_0]$ and p_0 are the stress tensor and the pore pressure at the reference state corresponding to $[\varepsilon] = [0]$ and $\varphi_j = 0$.

Considering an elastic matrix, dissolution process is the only source of energy dissipation. Thus Eq. (20) must be equal to zero when the dissolution process is not active, i.e. $\dot{n}_{M_i} = 0$.

Then, from local state postulate and by introducing the Legendre–Fenchel transform of W with respect to φ_j and $p_j - p_{j,0}$: $W^* = W - \varphi_j (p_j - p_{j,0})$ state equations read:

$$[\sigma] - [\sigma_0] = \frac{\partial W^*}{\partial[\varepsilon]}; \quad \varphi_j = -\frac{\partial W^*}{\partial(p_j - p_{j,0})} \tag{22}$$

Assuming isothermal evolutions, isotropic materials, and a quadratic form for W^*, the following constitutive equations of the solid matrix can be derived from skeleton states equations:

$$[\sigma] - [\sigma]_0 = E(V_M) : [\varepsilon] - \sum_{j=C,F} b_j(V_M, V_C)\left(p_j - p_{j,0}\right)[1] \tag{23}$$

$$\varphi_j = b_j(V_M, V_C)\varepsilon + \sum_{k=F,C} \frac{p_k - p_{k,0}}{N_{jk}(V_M, V_C)}; j = F, C \tag{24}$$

where $E:[\varepsilon] = (K - 2G/3)\varepsilon[1] + 2G[\varepsilon]$, with $\varepsilon = tr([\varepsilon])$, with $K = K(V_M)$ the bulk modulus of the cement skeleton, $G = G(V_M)$ its shear modulus, [1] the unity tensor and where the index 0 refers to the reference state.

Elastic parameters K and G are functions of the porosity created by the leaching process (e.g. V_M). A 3-phase model is used to estimate this dependency (e.g. [29]), which leads to the following expression for $K(V_M)$:

$$K(V_M) = \frac{4 G_m K_m (1 - \phi_0 - V_M)}{4G_m + 3K_m(\phi_0 + V_M)} \tag{25}$$

where K_m and G_m are respectively the bulk and shear moduli of the solid matrix. The expression of $G(V_M)$ can be found in [30].

As φ_j varies with S_j, it can be seen from Eq. (22) that b_j and N_{jk} depend on the cement matrix leaching V_M and the volume of carbonates V_C. Assuming that there is no morphological difference between the forming carbonate crystal and the in-pore fluid domains (they are both bounded by pores having the same shape) and that the deviation from the isodeformation condition remains negligible, this dependency can be estimated through [23,31]:

$$b_J = S_J b; \ b_F + b_C = b = 1 - \frac{K(V_M)}{K_m}$$

$$\frac{1}{N_{IJ}} = \frac{S_I S_J (b - \Phi)}{K_m}; \ \frac{1}{N_{FF}} + \frac{1}{N_{FC}} = \frac{b_F - (\Phi - V_C)}{K_m}; \ \frac{1}{N_{CC}} + \frac{1}{N_{FC}} = \frac{b_C - V_C}{K_m} \tag{26}$$

where b is the Biot modulus of the cement skeleton.

3.3. Conclusion on the influence of chemical reactions on poromechanical behaviour

In order to conclude on the influence of the chemical reactions on the poromechanical behaviour, we need to estimate the pore pressurisation induced by the carbonation process. To do so, the overall mass conservation of the in-pore fluid is considered:

$$\frac{1}{\rho_F}\frac{dm_F}{dt} = \frac{1}{\rho_F}\frac{d(\phi_F\rho_F)}{dt} = \frac{1}{\rho_F}\sum_{i=\alpha,w}\mathcal{M}_i\frac{dn_i}{dt} \tag{27}$$

where m_F is the mass of the in-pore fluid and $\mathcal{M}_i$ the molar mass of the phase $i = \alpha,w$. Using the combination of porosities' definitions, Eqs. (1)–(4), the continuity Eq. (13), and the in-pore fluid density evolution Eqs. (17) and (18), the mass conservation Eq. (27) becomes:

$$\frac{\phi_F}{K_F}\frac{dp_F}{dt} + \frac{d\varphi_F}{dt} = \sum_{i=\alpha,w}\overline{\nu}_i(\mathring{n}_i - \underline{\nabla}\cdot\underline{\omega}_i) - \mathring{V}_M + \mathring{V}_C \tag{28}$$

Finally, V_M and V_C expressions, Eq. (2), the molar quantities, Eqs. (14)–(15), and the expression of $\underline{\omega}_i$, Eq. (16), lead to:

$$\frac{\phi_F}{K_F}\frac{dp_F}{dt} + \frac{d\varphi_F}{dt} = \left(1 - \frac{\nu_{C,dis}}{\nu_C}\right)\mathring{V}_C - \sum_{M_i}\left(1 - \frac{\nu_{M_i,dis}}{\nu_{M_i}}\right)\mathring{V}_{M_i} \tag{29}$$
$$+ \nabla\cdot\left(\frac{\kappa}{\eta_F}\nabla p_F + d_{eff}\sum_{i=\alpha,w}\overline{\nu}_i\underline{\nabla}C_i\right)$$

where $\nu_{C,dis}$ and $\nu_{M,dis}$ are the molar volume of the dissolved carbonate crystal and of the matrix mineral M_i respectively:

$$\nu_{C,dis} = \overline{\nu}_{Ca^{2+}} + \overline{\nu}_{CO_3^{2-}} \text{ and } \nu_{Mi,dis} = \sum_{i=\alpha,w}\overline{\nu}_{i,M_i}a_{i,M_i} \tag{30}$$

Four phenomena contribute as the source terms of liquid pressure in Eq.(29). The term $-\sum_{M_i}\left(1 - \nu_{M_i,dis}/\nu_{M_i}\right)\mathring{V}_{M_i}$ corresponds to pressure relaxation due to the leaching of the cement matrix. $\left(1 - \nu_{C,dis}/\nu_C\right)\mathring{V}_C$ describes pressure increase/relaxation caused by the chemical reaction precipitation/dissolution of carbonates. $\nabla\cdot\left(d_{eff}\sum_{i=\alpha,w}\overline{\nu}_i\underline{\nabla}C_i\right)$ is the effect of the density change of in-pore water due to the migration of the dissolved species. Finally $d\varphi_F/dt$ is the term due to the porous network deformation, which is linked through Eq. (24) to the in-pore pressures, and to the porous medium strain, which in turn, satisfies the momentum balance equation:

$$\underline{\nabla}\cdot\left[\left(K - \frac{2}{3}G\right)\varepsilon[1] + G[\varepsilon] - \sum_J b_J p_J[1]\right] = \underline{0} \tag{31}$$

Considering the constitutive Eqs. (23)–(24), the in-pore pressurisation, Eq.(29), and momentum balance, Eq. (31), the model can quantify the influence of the chemical processes on the mechanical behaviour at the scale of a Representative Elementary Volume (i.e. millimetric scale) if the volume of precipitated carbonate and the leached matrix are known. In other words, it is sufficient to compute only the "major" chemical reactions, which engender variations of V_C and V_{Mi} in order to predict the mechanical impact of carbonation on a cement material.

However, it is impossible to know a priori the expression of these major reactions. Indeed, they are strongly dependent on the initial state of the system (mineralogy, fluid chemistry, initial pressure and temperature...) and may evolve during the solicitation. Then, the coupled workflow illustrated in Fig. 4 is proposed to solve the problem: First the major reactions and their validity domains (i.e. under which condition these reactions occur) are identified through reactive transport computations. Then, these reactions are imported
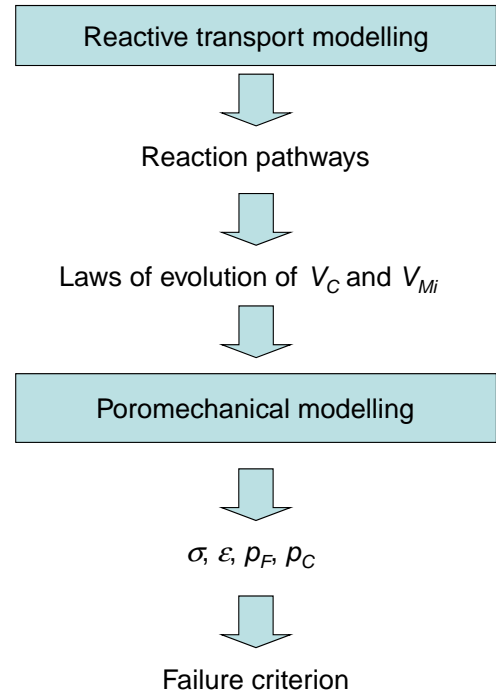

Fig. 4. Schematic representation of the link between the identified chemical processes and the poromechanical analysis.

into a mechanical code and used, when their validity domain is reached, to calculate the evolution of the chemical variables (i.e., V_C and V_{Mi}).

4. Application to a 1D cement carbonation problem

4.1. Description of the semi-analytical problem

In the following, a numerical application aimed at illustrating the chemo-mechanical coupling strategy is performed. Only the mechanical loading due to the carbonation process of a fully saturated one-dimensional structure made up of an isotropic medium, of length L and lateral surface S, ideally insulated on its lateral surfaces is considered. The Cartesian coordinate system O, x is used, with O the node of the surface, which is submitted to $\overline{CO}_2$ action and x following axis from the top to the bottom of the specimen. In this case, at the macroscopic scale, transport of fluid and species occurs only in the x direction, and the momentum balance Eq. (31) leads to the following analytical solution for the strain induced by carbonation process:

$$\varepsilon = \frac{f(t) + \sum_{j=F,C}b_J\left(p_j - p_{j,0}\right)}{K + 4G/3} \tag{32}$$

where $f(t)$ is a function of time that depends on the boundary conditions of the problem.

Substituting Eq. (32) in the constitutive Eq. (24) allows the following explicit expression of φ_F:

$$\varphi_F = S_F\left(\frac{b^2}{K + 4G/3} + \frac{1}{N}\right)(p_F - p_0 + S_C(p_C - p_F)) + f(t)\frac{S_F b}{K + 4G/3} \tag{33}$$

Consequently, only the fluid mass and in-pore species balance equations, accounting for the mechanical deformation through the analytical expression, Eq. (33), remains to be computed. In this context,
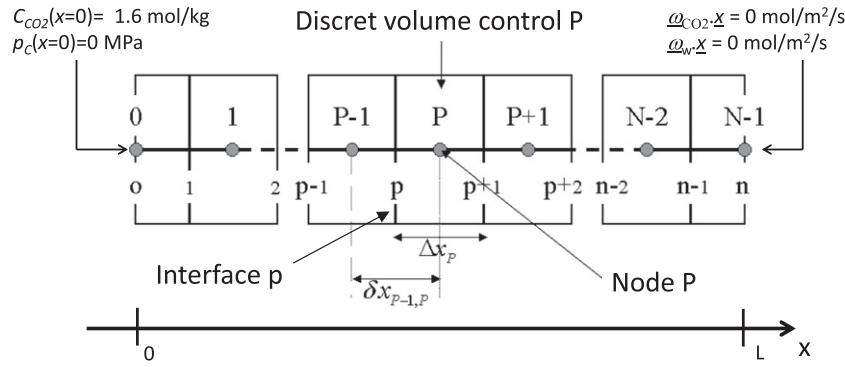
Fig. 5. Geometry and spatial discretization of the 1D model P and p respectively stand for the number of the discret volume control and for the number of the interface between the discret volume control P-1 and P.

a finite volume scheme (e.g. [32]) is used for numerical resolution of reactive-transport equations (Fig. 5).

Nevertheless, the developed poromechanical model is not restricted to this 1D case, its extension to 2D and 3D cases does not require any theoretical modification. However some numerical developments and adaptation of an appropriate numerical scheme are necessary to this end.

4.2. Initial and boundary conditions

The initial pressure and temperature conditions are isobaric and isothermal at $p_{CO2} = 280$ bar and $T = 80$ °C. At $t = 0$, the surface (i.e. $x = 0$) is submitted to 280 bar of supercritical CO_2 saturated by water. Under this condition, the dissolved CO_2 concentration of the in-pore water directly in contact with the supercritical CO_2 is close to 1.6 mol/kg of water, and the porous structure remains fully saturated. It is assumed that the carbonate crystal that solidifies at the $x = 0$ boundary is at the same pressure as the supercritical CO_2. So $p_C(x=0) = p_{CO2}$, while the mechanical boundary at $x = 0$ should be $[\sigma(x=0)] \cdot \underline{x} = -p_{CO2}\underline{x}$. At $x = L$, a no flow boundary ($\underline{\omega}_i \cdot \underline{x} = 0$, $i = w, \alpha$) is considered and the mechanical equilibrium is insured by a zero displacement boundary on the surface, leading to $f(t) = p_0 - p_{CO2}$ in Eq.(37), where p_0 is the pressure at the reference state. For this illustration, we will assume that the sample is at its reference state during the curing, which is made at the initial pressure and temperature conditions.

These boundary conditions are chosen in order to be as close as possible to a batch experiment such as the tests presented by [19,33]. In this experiment, a cylindrical sample of radius $R_s = 15$ mm is submitted to CO_2 penetration, leading to an axisymmetric carbonation of the specimen cross section. In order to reduce the differences between these experiments and the 1D simulation, the simulation is limited to a penetration front thickness lower than 10% of the specimen radius.

4.3. Estimation of model parameters

4.3.1. Identification of the reactions pathways

The "major" chemical reactions, which engender variations of V_C and V_{Mi}, are estimated through a reactive transport simulation performed by the code TOUGHREACT [34]. A simplified cement mineralogical system only composed by its two main constituents exposed in [35], namely Portlandite (CH) and hydrated calcium silicates (C–S–H,) is considered. A CH/C–S–H weight ratio equal to 0.36 in equilibrium with interstitial water free of dissolved carbonates is assumed. The secondary minerals are selected to account for calcite precipitation and C–S–H discretized decalcification from a C/S ratio = 1.6 to amorphous silica: C–S–H_1.6 → C–S–H_1.2 → C–S–H_0.8 → $SiO_{2(am)}$ (cf. Table 1).

The thermo-chemical properties used for the calculation are reported in Appendix C. Results, reported in Fig. 6, show that each cell begins to react when the upstream cell is fully carbonated. A sequence of four reactions between minerals and inward dissolved CO_2 (R_1 to R_4, Fig. 6) can be distinguished. Each of these reactions, reported in Table 2, can be written in the following global form:

$$R_i: \left(-a_{1,Ri}\right)M_{1,Ri} + CO_2 \rightarrow a_{2,Ri}M_{2,Ri} + a_{H_2O,R_i}H_2O + CaCO_3 \quad (34)$$
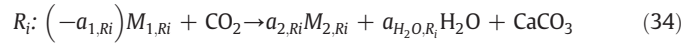
The reaction R_1 describes the CH carbonation while the reactions R_2 to R_4 describe the discrete carbonation of C–S–H leading to the leaving of amorphous silica + calcite.

As these reactions occur successively, it can be assumed that the advancement rate of the reaction R_i, noted $\dot{\xi}_{Ri}$ is null if the totality of mineral $M_{1,Ri}$ is dissolved or if the mineral $M_{1,Ri-1}$ is not yet totally dissolved. During dissolution of the mineral $M_{1,Ri}$, Eq. (34) leads to:

$$R_i: \dot{\xi}_{Ri} = \frac{\dot{n}_{M_{1,Ri}}}{a_{1,R_i}} = -\dot{n}_{CO_2} = \frac{\dot{n}_{M_{2,Ri}}}{a_{2,R_i}} = \frac{\dot{n}_{H_2O_{Ri}}}{a_{H_2O,R_i}} = \dot{n}_{C,R_i} \quad (35)$$

Consequently, for the present reaction sequences, Eqs. (14)–(15) can be written in the following form:

$$\dot{n}_C = \sum_{R_i} \dot{n}_{C,R_i} = \sum_{R_i} \dot{\xi}_{Ri}; \dot{n}_{M_i} = \sum_{R_i} \dot{n}_{M_i,R_i} = \sum_{R_i} a_{M_i,R_i} \dot{\xi}_{Ri} \quad (36)$$

For example, if we consider $M_i = $ C–S–H_0.8, its mole variation is $\dot{n}_{C-S-H\_0.8} = 1.25\,\dot{\xi}_{R_3} - 1.25\,\dot{\xi}_{R_4}$.

Moreover, the calculation reported in Fig. 6 underlines that the incoming CO_2 within the cell is totally consumed through this sequence. Consequently, the advancement rate of the reactions R_1 to R_4 can be estimated from the amount of incoming $CO_{2(aq)}$ in a given cell.

4.3.2. Calibration of initial transport properties

Permeability and effective diffusivity are the key parameters of the developed model as they govern the kinetics of carbon penetration within the porous medium (Eq. (16)) and pressure relaxation

Table 1
Formula of the minerals considered in the chemical system.

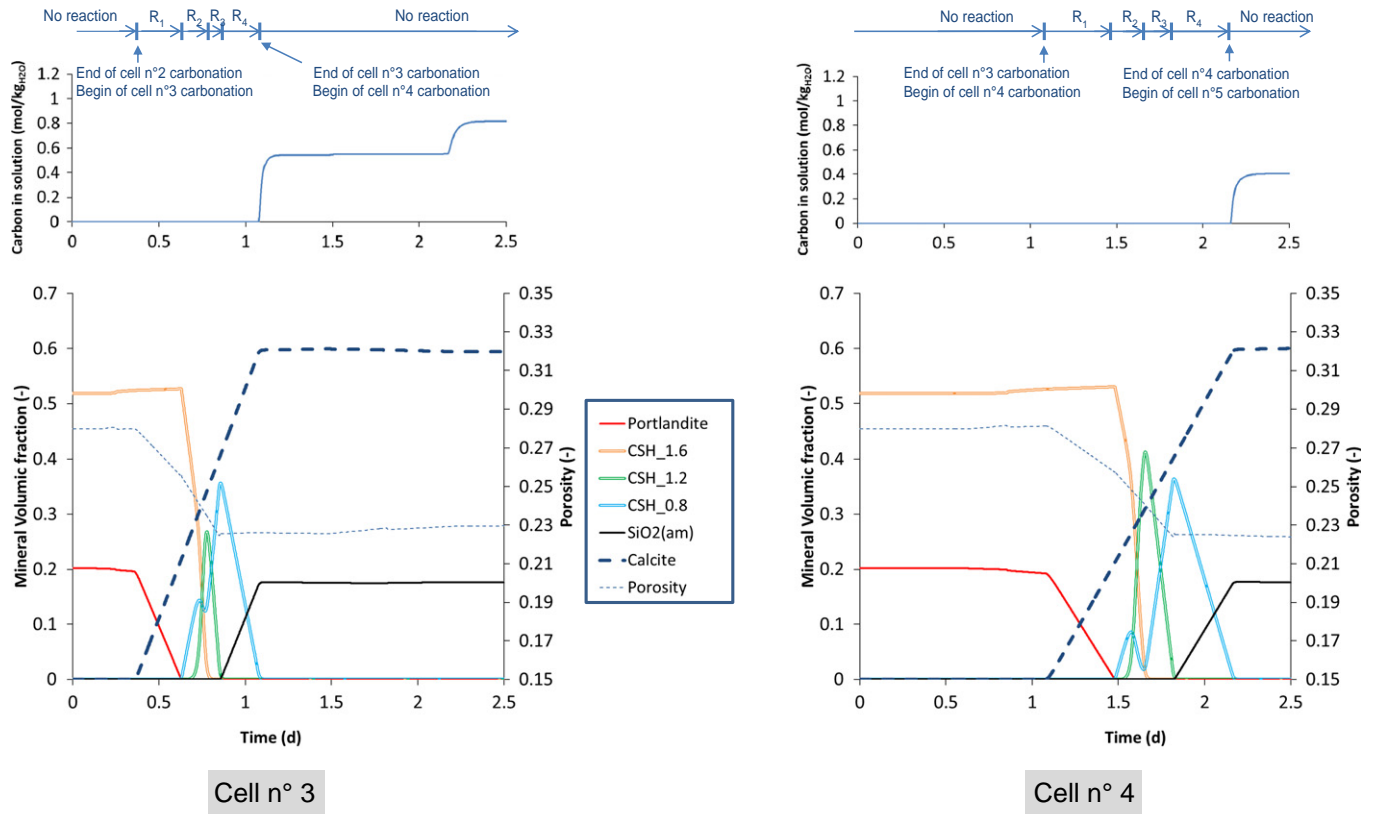| Mineral	Structural formula
Portlandite	$Ca(OH)_2$
CSH_1.6	$Ca_{1.60}SiO_{3.6}{:}2.58H_2O$
CSH_1.2	$Ca_{1.2}SiO_{3.2}{:}2.06H_2O$
CSH_0.8	$Ca_{0.8}SiO_{2.8}{:}1.54H_2O$
$SiO_{2(am)}$	SiO_2
Calcite	$CaCO_3$

Fig. 6. Computation with TOUGHREACT of the temporal evolutions of mineral volumes within two adjacent cells. R1 to R4 refer to the reactions Ri described in Table 2.

Table 2

Identification of the reactions pathway that drives the carbonate precipitation and the matrix leaching during the carbonation process.

Ri	$a_{1,Ri}$	$M_{1,Ri}$	$+ CO_2$	$\rightarrow$	$a_{2,Ri}$	$M_{2,Ri}$	$+ CaCO_3$	$+ a_{H2O,Ri}$	H_2O
R_1	1	$Ca(OH)_2$	$+ CO_2$	$\rightarrow$	0	0	$+ CaCO_3$	$+ 1$	H_2O
R_2	2.5	$CSH\_1.6$	$+ CO_2$	$\rightarrow$	2.5	$CSH\_1.2$	$+ CaCO_3$	$+ 1.3$	H_2O
R_3	2.5	$CSH\_1.2$	$+ CO_2$	$\rightarrow$	2.5	$CSH\_0.8$	$+ CaCO_3$	$+ 1.3$	H_2O
R_4	1.25	$CSH\_0.8$	$+ CO_2$	$\rightarrow$	1.25	$SiO_{2(am)}$	$+ CaCO_3$	$+ 1.925$	H_2O

(Eq. (29)). The permeability–porosity relation reported by [36], which seems to fit with experimental results from [19] and [37] (cf. Fig. 7A), is used to estimate the intrinsic permeability of class G cement:

$$\kappa = 1.2 \times 10^{-19} \left(\frac{\phi_F}{0.26} \right)^{11} \tag{37}$$

To our knowledge, no clear experimental relation exists to estimate the effective diffusivity for class G cement. In addition the effective diffusivity varies with temperature, viscosity, species that migrates, etc. In the present work, this parameter is estimated from
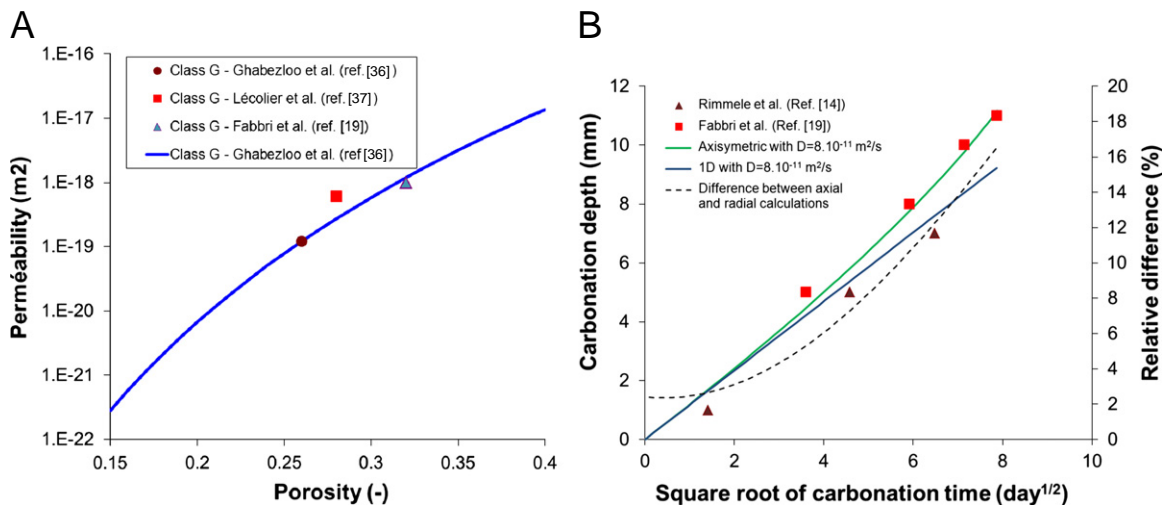

Fig. 7. (Graph A): Comparison between the κ–ϕ relation from [36] with experimental data on class G cements. (Graph B): Comparison between the rate of progress of carbonation front from [19] and [14] with the rate estimated from this work for $D = 8E^{-11}$ m²/s.

Table 3
Values of κ and d_{eff} used for the parametric analysis.

Case	a	b	c
d_{eff}/κ	δ_0	$10\,\delta_0$	$\delta_0/10$
$\kappa_{\phi=0.28}$ (m^2)	$2.7\,10^{-19}$	$1.35\,10^{-19}$	$5.4\,10^{-19}$
d_{eff} (m^2/s)	$8\,10^{-11}$	$40\,10^{-11}$	$1.6\,10^{-11}$

the comparison between the carbonation depth observed from the batch experiences [19] and the one predicted by a radial reactive-transport simulation (see Fig. 7B).

This simulation considers a total radius R_s of 15mm and the assumptions, mineralogy and boundaries reported in previous paragraphs. The depth of the penetration front is then estimated from the thickness of the cells that are totally carbonated (only composed by amorphous silica and calcite). An effective diffusivity coefficient equal $d_{eff} = 8.0\,10^{-11}$ m²/s is finally considered. It is worth noting that the aforementioned calibration includes important approximations. Indeed, the value of the effective diffusivity depends on the model assumption. Moreover, as previously underlined by [17], the validity of a simple model based on the Fick law to describe the penetration of ingress species is questionable due to the drastic modification of the mineral assemblage during the carbonation process.

Reactive transport simulations are performed in the same conditions but for the geometry defined in §4.1 to verify the 1D assumption. This comparison, reported in Fig. 7B, underlines that for a front penetration lower that 10% of the sample radius, the difference between the 1D and axisymmetric simulations remains negligible (lower than 3%).

4.3.3. Evolution of the transport properties with carbonation

The permeability measurements realised by [19] on a sample at different stages of carbonation show that the carbonation process leads to a significant decrease of permeability. This result is not surprising as intrinsic permeability is known to be strongly influenced by larger connected pores, which are totally sealed by carbonates during the process. Eq. (37) is used to take into account this effect.

On the contrary, no clear relation is established between carbonation and effective diffusion coefficient (e.g. [38]). Actually, effective diffusivity is known to be rather dependent on capillary porosity (pore size lower than 100 nm), which is less influenced by carbonation process than large pores. However, it is difficult to make any quantitative conclusion from this qualitative remark and a precise determination of this coefficient and its evolution during carbonation remains a major issue for the accurate modelling of interaction between cement and CO_2[17]. Consequently, a constant d_{eff} is assumed in the following, and the effect of the variability of d_{eff} on the results is rather investigated through a sensibility analysis.

4.4. Calculation of the mechanical impact of the carbonation process

Regarding the reaction pathways reported in Table 2, the combination between $\mathring{V}_C$ and $\mathring{V}_{M_i}$, given by Eq. (2), and the mole variation, given by Eq. (36), allows the evaluation of the chemical overpressure source as:

$$\left(1 - \frac{v_{C,dis}}{v_C}\right)\mathring{V}_C - \sum_{M_i}\left(1 - \frac{v_{M_i,dis}}{v_{M_i}}\right)\mathring{V}_{M_i} + \nabla\cdot\left(d_{eff}\sum_{i=\alpha,w}\overline{v}_i\nabla C_i\right) \quad (38)$$
$$= \sum_{R_i}\Delta v_{R_i}\mathring{\xi}_{R_i} + \overline{v}_{CO_2}\frac{dn_{CO_2}}{dt}$$

where $\Delta v_{R_i} = v_C + a_{M_2,R_i}v_{M_2,R_i} + a_{H_2O,R_i}v_{H_2O} + a_{M_1,R_i}v_{M_1,R_i}$ and $\mathring{\xi}_{R_i}$ is the advancement rate of reaction R_i.

Then, accounting for the φ_F expression reported in Eq. (33), the substitution of Eq. (38) in the in-pore pressure variation (Eq. (29)),

leads to the following simplified expression for the in-pore pressurisation:

$$\frac{d}{dt}\left(\frac{p_F}{L_F}\right) + \frac{d}{dt}\left(\frac{p_C - p_F}{L_{FC}}\right) = \sum_{R_i}\Delta v_{R_i}\mathring{\xi}_{R_i} + \overline{v}_{CO_2}\frac{dn_{CO_2}}{dt} + \nabla\cdot\left(\frac{\kappa}{\eta_F}\nabla p_F\right) \quad (39)$$

where $1/L_F = \phi_F/K_F + S_F(b^2/(K+4G/3) + 1/N)$, and $1/L_{FC} = S_C S_F(b^2/(K+4G/3) + 1/N)$.

As previously discussed, $\mathring{\xi}_{R_i}$ can be estimated from the amount of carbon entering each cell. Thus, using Eqs. (13) and (16) we can write:

$$\mathring{\xi}_{Ri} = \begin{cases} \nabla\cdot\left(d_{eff}\nabla\left(\frac{n_{CO_2}}{\phi_F}\right) + \left(\frac{n_{CO_2}}{\phi_F}\right)\frac{\kappa}{\eta_F}\nabla p_F\right) \text{ if } M_{1,R_i}\neq 0 \text{ and } M_{1,R_{i-1}} = 0 \\ 0 \text{ otherwise} \end{cases} \quad (40)$$

$$\frac{dn_{CO_2}}{dt} = \nabla\cdot\left(d_{eff}\nabla\left(\frac{n_{CO_2}}{\phi_F}\right) + \left(\frac{n_{CO_2}}{\phi_F}\right)\frac{\kappa}{\eta_F}\nabla p_F\right) - \sum_{R_i}\mathring{\xi}_{R_i}$$

This 1D non-linear problem, Eqs. (39)–(40), is solved within the finite volume approach described previously. The calculation is made considering the values of κ and d_{eff} reported in Table 3 and the following material parameters: $K_m = 17.5$ GPa [41], $G_m = 10$ GPa (indirectly estimated from the skeleton shear modulus reported in [42]), $K_F = 2.2$ GPa [39] and $K_C = 70$ GPa [40]. Numerical values used for the other thermo-mechanical parameters are reported in Appendix C.

5. Results and discussion

Fig. 8A shows the fluid and carbonate pressure profiles' evolutions during the first 35 h of carbonation. It can be seen that for an effective diffusion coefficient of $8.0\,10^{-11}$ m²/s, the calculation leads to a reduction of the fluid pressure due to the capillary effect and a small crystal over-pressure (29 MPa versus 28 MPa of confining pressure) within the confined pore space. Even if this over-pressure seems not to be sufficient in order to damage the solid matrix, it may contribute to its embrittlement when combined with others phenomena. However, the interpretation of these results should be made with care as great uncertainties exist on d_{eff} and, in a less important extent, on κ. To scan the effect of these variations and uncertainties, a parametric study is carried out considering several values of the d_{eff}/κ_0 ratio (called δ in the following) ranging from $10\,\delta_0$ to $\delta_o/10$ (cf. Table 3), where δ_0 is the d_{eff}/κ_0 ratio corresponding to the values considered for the reference case, and κ_0 is the initial permeability for $\phi_F = \phi_0$.

The results, reported in the Fig. 8B, are compared for the same carbonation depth of 1.35 mm (and not at the same time). These calculations show that for a higher effective diffusivity coefficient and/or a lower permeability, the pore overpressure increases significantly. In fact, the carbonation process tends to reduce the effective porous volume: the density of cement matrix that is leached is higher than the density of carbonate crystals that precipitates. As it was emphasized by [19] at the pore scale, in case of low permeable cements or in case of fast porous volume variation, the liquid flow expulsion will not be enough important to relax the whole local overpressure caused by this porous volume reduction. This is why, for higher d_{eff}/κ ratio, localized fluid overpressure is obtained at the carbonation front, where the porous volume variation rate is more important.

However, the knowledge of the pore pressures and strain is not sufficient to estimate the susceptibility of the solid matrix to be damaged. A failure criterion must be considered to go further in this discussion. In the present study, a brittle damage, caused by a pore overpressurisation, is expected at the carbonation front. In this context, we can use the brittle failure criterion reported in [22]:
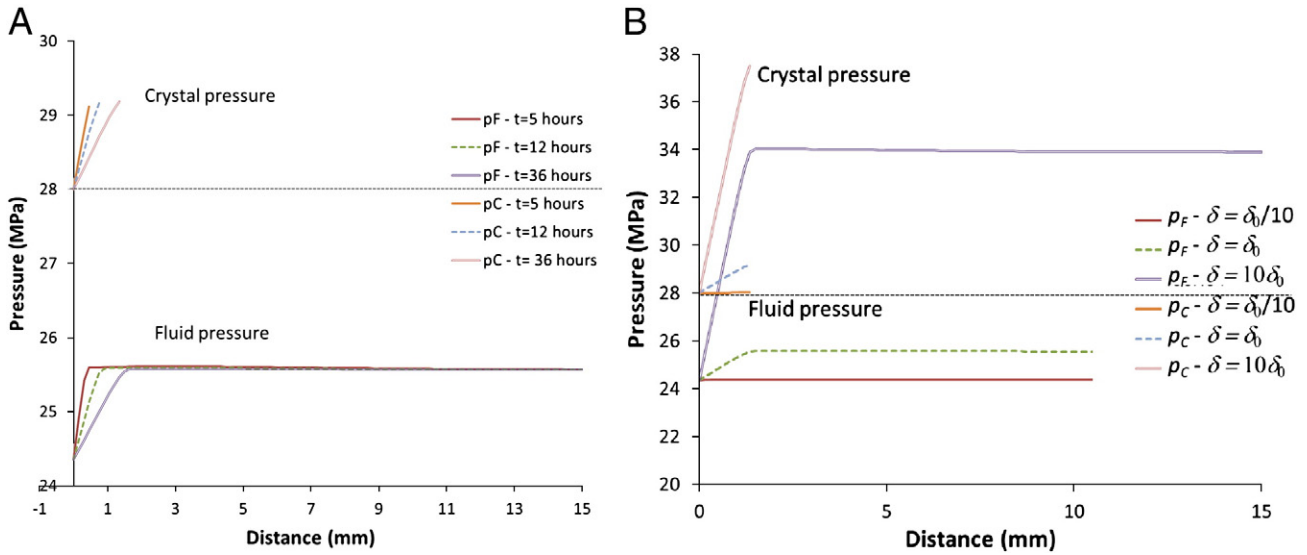
$$\frac{W}{W_{cr}} \leq 1 \quad (41)$$

Fig. 8. Evolution of in-pore pressures during (A) the first 35 h of carbonation and (B) for several $\delta = d_{eff}/\kappa$ ratio at the same carbonation depth (1.35 mm).

where W is the elastic free energy of the solid matrix introduced in §3.2, while W_{cr} is the threshold energy that can accumulate the solid matrix before being damaged. Neglecting the chemical energy associated with the chemical bound in the non-deformed state, the constitutive Eqs. (23–24) allow to write the elastic energy stored within the solid matrix (W):

$$W = \frac{\left(\Delta\sigma + \sum_{i=C,F} b_i \Delta p_i\right)^2}{2K} + \sum_{i,j=C,F} \frac{\Delta p_i \Delta p_j}{2N_{ij}} + \frac{\Delta[\sigma]_D : \Delta[\sigma]_D}{4G} \quad (42)$$

where ΔX stands for $X - X_0$, σ for the mean stress and $[\sigma]_D$ for the deviatoric stress tensor. This criterion is independent of the solicitation that produces the pore pressure increase as it is only based on the matrix energy. Then, W_{cr} can be estimated from the free energy dissipated during the failure of a specimen submitted to an isotropic loading tests, which is close to 2 kPa in tension and to 20 kPa in compression for a W/C = 0.4 Portland cement (adapted from [43]). The calculation of W/W_{cr} at the carbonation front for different values of κ/d_{eff} ratios and for the same carbonation depth is reported in Fig. 9. For $d_{eff}/\kappa = \delta_0$, the value of W/Wcr at the carbonation front is equal to 0.02. Consequently, even if
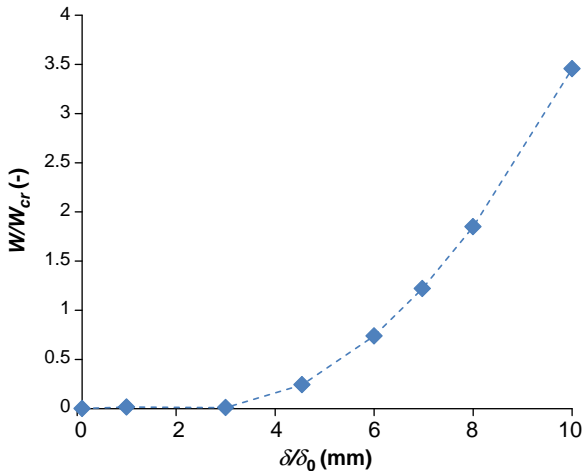

Fig. 9. Evolution of W/W_{cr} at the carbonation front for $\delta = d_{eff}/\kappa$ ratios ranging from $\delta_0/10$ to $10\delta_0$ and for a carbonation depth of 1.35 mm.

the carbonation process produces an overpressure of carbonate, it should not be sufficient to damage the cement matrix. However, as sketched in Fig. 9, even small variation in δ may lead to important variations in W/Wcr: The critical value of $W/W_{cr} = 1$ is exceeded for $\delta = 7\delta_0$, which is in the range of uncertainty of the measurements, estimation of both permeability and diffusivity coefficients, and in the range of possible values for cement based materials.

Due to approximations considered in this simulation (simplified mineralogy, chemical equilibrium, poro-elastic modelling...) and the uncertainties of input parameters (effective diffusivity, permeability...), these results should not be understood in a quantitative way. Nevertheless, they show that the carbonate precipitation may have an important impact on the mechanical stability of a cementitious medium. Especially on the carbonation front where pore overpressure which might lead, under specific condition, to material failure. Even if a direct comparison is not possible, these results follow the same trends as the experimental observation made by [19] where damage at carbonation front is observed on cement sample carbonated under comparable conditions.

In addition, this calculation confirms that the risk of damage increases when d_{eff}/κ ratio is high. This may be the case, for example, for cements with low W/C ratio (lower than 0.4) with a large amount of connected capillary and gel pores (pore diameter lower than 100 nm) but with practically no connected macropores [44]. This kind of porous network geometry commonly leads to a very low permeability regarding cements with a higher W/C ratio. Meanwhile, the connected network of capillary pores allows a relatively high effective diffusion coefficient. So, these cements may be much more influenced by carbonation induced damage than more porous and permeable ones despite their grater mechanical resistance.

Finally, it must be mentioned that for a complete study of the integrity of the cement structure, at least all the chemical, thermal and mechanical solicitations of the cement (e.g. reservoir pressurisation and thermal variation, *in-situ* stress anisotropy, etc.) should be investigated to obtain a reliable conclusion.

6. Conclusion

A method to estimate the influence of the chemical processes involved during a wellbore cement carbonation on its mechanical behaviour is developed. The main advantage of this method is to take only into account the major chemical reactions, identified from a reactive transport pre-calculation. Then, the calculation times are drastically reduced. Moreover,

the poromechanic framework used here allows the identification of the main overpressure sources and thus the main processes that solicitate the solid matrix and to quantify their actions on the material integrity.

Even the assumptions made in this study do not allow to conclude on the *in-situ* mechanical stability of the wellbore cement, the preliminary results of the poromechanical model show that under particular κ and d_{eff} values, the carbonation process significantly impacts the mechanical behaviour, and thus, damage can occur. The next step of this study should be the implementation of this model into a 2D/3D large scale numerical simulation tool in order to estimate the influence of these chemical reactions under a more realistic geological storage context.

Acknowledgements

Appendix A. List of symbols and their [unit]

Latin letters

$a_{j,Mi}$	stoichiometric coefficient of the species j in the dissolution/precipitation reaction of the mineral M_i [−]
b_C, b_F	Partial Biot coefficient associate to resp. the in-pore fluid and the carbonate [−]
C	Carbonate crystal
C_i	Molar concentration of the species i [mol/m^3]
C_{FC}	Curvature of the fluid–carbonate interface [m]
d_{eff}	Effective diffusion coefficient [m^2/s]
F	In-pore fluid
G	Shear modulus of the skeleton [Pa]
K, K_C, K_F, K_m	Bulk moduli of resp. the skeleton, the carbonates, the in-pore fluid and the solid matrix [Pa]
m_F	Fluid mass per unit of VER volume [kg/m^3]
M_i	Solid mineral other that carbonate
$\mathcal{M}_i$	Molar mass of i [kg/mol]
n_i	Molar quantity of the phase i per unit of VER volume [mol/m^3]
$\dot{n}_i$	Mole variation of i due to chemical reactions [mol/m^3/s]
N_{ij}	Partial Biot modulus associate to the phases i and j [Pa]
p_a, p_o, p_F, p_C	Resp. average, reference, fluid and carbonate pressures [Pa]
S_F, S_C	Lagrangian saturation ratio of in-pore fluid (F) or carbonate (C) [−]
V_M, V_C	Volume of matrix leached and carbonate precipitated per unit of Ω_0 [−]
w	Water molecule (H_2O)
W, W^*	Resp. free and complementary energy of the matrix [Pa]
W_{cr}	Critical free energy leading to a tensile brittle failure [Pa]

Greek letters

α	Dissolved ionic species (e.g. a = Ca^{2+}, CO_3^{2-}, OH^-, etc.)
δ	Ratio between effective diffusivity and initial permeability [s^{-1}]
$[\varepsilon]$	Strain tensor [−]
ε	Volumetric strain [−]
ϕ, ϕ_0	Current or initial overall porosity [−]
ϕ_F, ϕ_C	Current porosity filled by resp. fluid or carbonates [−]
φ_F, φ_C	Deformation of the porosity filled by resp. in-pore fluid or carbonates [−]

Φ	Current overall porosity prior any deformation [−]
γ_{FC}	Surface tension of the fluid–carbonate interface [N/m]
η_F	Dynamic viscosity of the in-pore fluid [Pa s]
κ	Intrinsic permeability [m^2]
μ_i	volumetric chemical potential of i [J/mol]
ν_{Mi}	Molar volume of the mineral M_i [m^3/mol]
$\bar{v}_i$	Partial molar volume of species i [m^3/mol]
$\nu_{C,dis} \nu_{Mi,dis}$	Molar volume of resp. dissolved carbonate and mineral M_i [m^3/mol]
Ω_0	Initial volume of the REV [m^3]
ρ_F, ρ_C	Density of resp. in-pore fluid or carbonates [kg/m^3]
$[\sigma], [\sigma_0]$	Stress tensor resp. at current or reference state [Pa]
ω_i	mole transport of phase i [mol/m^2/s]
ξ_{Ri}	Advancement of the reaction R_i [mol/m^3]

Appendix B

The starting point of this demonstration is the classical Clausius–Duhem relation, reported, for example in [28]:

$$[\sigma]: \frac{d[\varepsilon]}{dt} - \sum_{i=\alpha,w} \mu_i \underline{\nabla} \cdot \underline{\omega_i} - \frac{d\Psi}{dt} \geq 0 \tag{B.1}$$

where $[\sigma]$ and $[\varepsilon]$ are the stress and strain tensors, while $\underline{\omega_i}$ and μ_i are the molar flow and the chemical potential of phase $i = \alpha, w$. From Eqs. (13)–(16), we can write:

$$\sum_{i=\alpha,w} \mu_i \underline{\nabla} \cdot \underline{\omega_i} = -\dot{n}_C \left(\mu_{Ca^{2+}} + \mu_{CO_3^{2-}} \right) - \sum_{M_i} \left(\dot{n}_{M_i} \sum_j a_{j,M_i} \mu_j \right) - \sum_{i=\alpha,w} \mu_i \frac{dn_i}{dt} \tag{B.2}$$

Ψ is the free energy of the porous medium. It is the sum of the free energies of the cement skeleton, Ψ_s, the carbonate crystal, $\Psi_C = n_C \mu_C - \phi_C p_C$ and the in-pore solution constituent, $\Psi_F = (\sum_{i=\alpha,w} n_i \mu_i) - \phi_F p_F$. From this partition, the use of Gibbs–Duhem relations (Eqs. (7)–(8)) and of the mole balance relation of the carbonate crystal (i.e. $dn_C / dt = -\dot{n}_{C\rightarrow}$) leads to:

$$\frac{d\Psi}{dt} = \frac{d\Psi_s}{dt} + \sum_{i=\alpha,w} \mu_i \frac{dn_i}{dt} + \mu_C \dot{n}_C - \sum_{J=F,C} p_J \frac{d\phi_J}{dt} \tag{B.3}$$

By substituting Eqs. (B.2) and (B.3) in Eq. (B.1) we get:

$$[\sigma]: \frac{d[\varepsilon]}{dt} + \dot{n}_C \left(\mu_{Ca^{2+}} + \mu_{CO_3^{2-}} - \mu_C \right) + \sum_{M_i} \left(\dot{n}_{M_i} \sum_j a_{j,M_i} \mu_j \right)$$
$$+ \sum_{J=F,C} p_J \frac{d\phi_J}{dt} - \frac{d\Psi_s}{dt} \geq 0 \tag{B.4}$$

Assuming that the carbonate, solid matrix and in-pore water are at the equilibrium at each point (or in the whole model) and at any time, the injection of Eqs. (6) and (12) in Eq. (B.4) allows:

$$[\sigma]: \frac{d[\varepsilon]}{dt} + \sum_{M_i} \mu_{M_i} \dot{n}_{M_i} + \sum_{J=F,C} p_J \frac{d\phi_J}{dt} - \frac{d\Psi_s}{dt} \geq 0 \tag{B.5}$$

Under this definition, we can write:

$$p_C \frac{d\phi_C}{dt} + p_F \frac{d\phi_F}{dt} = p_a \dot{V}_M + \sum_J p_J \frac{d\varphi_J}{dt} + \Phi(p_C - p_F) \frac{dS_C}{dt} \tag{B.6}$$

where p_a is the average pore pressure, defined by:

$$p_a = S_F p_F + S_C p_C \tag{B.7}$$

Then, the combination of Eqs. (B.5)–(B.7) and the use of Eq. (2) lead to:

$$[\sigma]: \frac{d[\varepsilon]}{dt} - \sum_{M_i} \left(v_{M_i} p_a - \mu_{M_i} \right) \mathring{n}_{M_i} + \Phi(p_C - p_F) \frac{dS_C}{dt} + \sum_{J=F,C} p_J \frac{d\varphi_J}{dt} - \frac{d\Psi_s}{dt} \geq 0 \tag{B.8}$$

Considering an elastic matrix, the only source of dissipation is the dissolution process. Thus Eq. (B.8) must be equal to zero when the dissolution process is not active, i.e. for $\mathring{n}_{M_i} = 0$.

From local state postulate, we conclude that the state equations read:

$$[\sigma] = \frac{\partial \Psi_s}{\partial [\varepsilon]}; p_J = \frac{\partial \Psi_s}{\partial \varphi_J}; \Phi(p_C - p_F) = \frac{\partial \Psi_s}{\partial S_C} \tag{B.9}$$

Let us emphasize that liquid–crystal, liquid–matrix and crystal–matrix interfaces possess their own proper interfacial energy and entropy. This energy will be noted ΦU and is supposed to not depend on the skeleton deformation.

On the other side, the free energy of the matrix, W, is only a function of skeleton strain, elastic porosity deformation, and leaching. The free energy of the skeleton can thus be expressed as:

$$\Psi_s\left([\varepsilon], \varphi_J, S_C, \Phi\right) = p_0 \Phi + [\sigma_0]: [\varepsilon] + W\left([\varepsilon], \varphi_J, V_M\right) + \Phi U\left(S_C, \varphi_J\right) \tag{B.10}$$

where p_0 and $[\sigma_0]$ stand for the reference state pressure and stress tensor. Substitution of Eq. (B.10) into the state Eq. (B.9), provides the remaining state equations:

$$[\sigma] - [\sigma_0] = \frac{\partial W}{\partial [\varepsilon]}; \quad \overline{p_J} - p_0 = \frac{\partial W}{\partial \varphi_J}; \quad \Phi(p_C - p_F) = \frac{\partial(\Phi U)}{\partial S_C} \tag{B.11}$$

where $\overline{p_J} = p_J - \partial(\Phi U)/\partial \varphi_J$ is the pressure effectively transmitted to the cement matrix through the internal solid walls delimiting the porous volume occupied by constituent J. Using multi-scale techniques, as reported in [45], it can be shown that $\partial(\Phi U)/\partial \varphi_J$ can be neglected if S_C is higher than 0.1. Thus, in case of the saturated carbonation process, this term can be neglected. Under these notations and assumptions, Eq. (B.8) can be written in the form:

$$([\sigma] - [\sigma_0]): \frac{d[\varepsilon]}{dt} - \sum_{M_i} \left(v_{M_i}(p_a - p_0) - \mu_{M_i} \right) \mathring{n}_{M_i} + \sum_{J=F,C} \left(p_J - p_0 \right) \frac{d\varphi_J}{dt} - \frac{dW}{dt} \geq 0 \tag{B.12}$$

Appendix C. Thermophysical properties

The computations are made with $v_{Ca(OH)2} = 33.1$ cm³/mol, $v_{CSH1.6} = 84.7$ cm³/mol, $v_{CSH1.2} = 72$ cm³/mol, $v_{CSH0.8} = 59.3$ cm³/mol, $v_{SiO2} = 29$ cm³/mol, $v_{CaCO3} = 39.6$ cm³/mol, $v_{CO2} = 20.8$ cm³/mol, $v_{H2O} = 18.3$ cm³/mol [46] and $\phi_0 = 0.28$. There is an evolution of the viscosity with ionic concentration. In this study, we used the empirical relation proposed by [47] to scan this effect:

$$\frac{\eta_F^0 - \eta_F}{\eta_F^0} = 4.65 x_{CO_2} \tag{C.1}$$

where x_{CO2} is the molar fraction of dissolved CO_2 and η_F^0 is the viscosity of water equal to 0.36 mPa s at 80 °C. Finally, the equilibrium constant

used for identification of the reaction pathways, is taken from the database THERMODDEM [46] and is reported in the following table:

Equilibrium	Log K at 80 °C
Gas dissolution–dissociation	
$CO_{2(g)} + H_2O \Leftrightarrow HCO_3^- + H^+$	−8.217
Speciation in water	
$Ca(HCO_3)^+ \Leftrightarrow Ca^{2+} + HCO_3^-$	−1.106
$CaCO_{3(aq)} + H^+ \Leftrightarrow Ca^{2+} + HCO_3^-$	6.336
$CaOH^+ + H^+ \Leftrightarrow Ca^{2+} + H_2O$	10.697
$CO_{2(aq)} + H_2O \Leftrightarrow H^+ + HCO_3^-$	−6.329
$CO_3^{2-} + H^+ \Leftrightarrow HCO_3^-$	10.064
$H_2SiO_4^{2-} + 2\,H^+ \Leftrightarrow H_4SiO_{4(aq)}$	21.422
$HSiO_3^- + H^+ + H_2O? \Leftrightarrow H_4SiO_{4(aq)}$	9.146
$OH^- + H^+ \Leftrightarrow H_2O$	12.641
Mineral dissolution/precipitation	
$Portlandite + 2\,H^+ \Leftrightarrow Ca^{2+} + 2\,H_2O$	19.288
$Calcite + H^+ \Leftrightarrow Ca^{2+} + 2\,HCO_3^-$	1.079
$CSH\_1.6 + 3.2\,H^+ \Leftrightarrow 1.6\,Ca^{2+} + H_4SiO_{4(aq)} + 2.18\,H_2O$	24.453
$CSH\_1.2 + 2.4\,H^+ \Leftrightarrow 1.2\,Ca^{2+} + H_4SiO_{4(aq)} + 1.26\,H_2O$	16.950
$CSH\_0.8 + 1.6\,H^+ \Leftrightarrow 0.8\,Ca^{2+} + H_4SiO_{4(aq)} + 0.34\,H_2O$	9.794
$Amorphous\ silica + 2\,H_2O \Leftrightarrow H_4SiO_{4(aq)}$	−2.337

References

[1] S. Pacala, R. Socolow, Stabilization wedges: solving the climate problem for the next 50 years with current technologies, Science 305 (2004) 968.

[2] IPCC, IPCC Special Report on Carbon Dioxide Capture and Storage. Prepared by Working Group III of the Intergovernmental Panel on Climate Change, in: B. Metz, O. Davidson, H.C. de Coninck, M. Loos, L.A. Meyer (Eds.), Cambridge University Press, Cambridge, United Kingdom/New York, USA, 2005.

[3] S. Benson, P. Cook, et al., Chapter 5: Underground Geological Storage *in* IPCC Special Report on Carbon Dioxide Capture and Storage, 2005, pp. 197–265.

[4] ADEME, BRGM, IFP, CO_2 capture and storage in the subsurface, in: I. Czernichowski-Lauriol, A. Ehinger, N. Thybaud (Eds.), Geoscience Issues, 2007, 64 p.

[5] K. Pruess, J. García, Multiphase flux dynamics during CO_2 disposal into saline aquifers, Environmental Geology 48 (2002) 282–295.

[6] I. Gauss, P. Audigane, L. André, J. Lion, N. Jacquemet, P. Durst, I. Czernichowski-Lauriol, M. Azaroual, Geochemical and solute transport modelling for CO_2 storage, what to expect from it? International Journal of Greenhouse Gas Control 2 (2008) 605–625.

[7] J. Rutqvist, J.T. Birkholzer, C. Tsang, Coupled reservoir–geomechanical analysis of the potential for tensile and shear failure associated with CO_2 injection in multilayered reservoir–caprock systems, International Journal of Rock Mechanics and Mining Science 45 (2008) 132–143.

[8] J. Rohmer, D.M. Seyedi, Coupled large scale hydromechanical modelling for caprock failure risk assessment of CO_2 storage in deep saline aquifers, Oil & Gas Science and Technology − Revue d'IFP 65 (2010) 503–517, doi:10.2516/ogst/2009049.

[9] O. Bouc, P. Audigane, G. Bellenfant, H. Fabriol, M. Gastine, J. Rohmer, D. Seyedi, Determining safety criteria for CO_2 geological storage, Energy Procedia 1 (2009) 2439–2446.

[10] V. Barlet-Gouédard, G. Rimmelé, B. Goffé, O. Porcherie, Well technologies for CO_2 geological storage: CO_2-resistant cement, Oil & Gas Science and Technology 62 (2007) 325–334.

[11] N. Jacquemet, J. Pironon, E. Caroli, A new experimental procedure for simulation of $H_2S + CO_2$ geological storage. Application to well cement aging, Oil and Gas Science and Technology 60 (1) (2005) 193–206.

[12] N. Jacquemet, J. Pironon, J. Saint-Marc, Mineralogical changes of a well cement in various H_2S–CO_2(−brine) fluids at high pressure and temperature, Environment Science and Technology 42 (2008) 282–288.

[13] B.G. Kutchko, B.R. Strazisar, N. Huerta, G.V. Lowry, D.A. Dzombak, N. Thaulow, CO_2 reaction with hydrated class H well cement under geologic sequestration conditions: effects of flyash admixtures, Environmental Science and Technology 43 (10) (2009) 3947–3952.

[14] G. Rimmelé, V. Barlet-Gouédard, O. Porcherie, B. Goffé, F. Brunet, Heterogeneous porosity distribution in Portland cement exposed to CO_2-rich fluids, Cement and Concrete Research 38 (2008) 1038–1048.

[15] A. Duguid, G.W. Scherer, Degradation of oilwell cement due to exposure to carbonated brine, International Journal of Greenhouse Gas Control 4 (2010) 546–556.

[16] W. Crow, J.W. Carey, S. Gasda, D.B. Williams, M. Celia, Wellbore integrity analysis of a natural CO_2 producer, International Journal of Greenhouse Gas Control 4 (2010) 186–197.

[17] B.M. Huet, J.H. Prevost, G.W. Scherer, Quantitative reactive transport modeling of Portland cement in CO_2-saturated water, International Journal of Greenhouse Gas Control 4 (2010) 561–574.

[18] F. Gherardi, P. Audigane, E.C. Gaucher, Predicting long-term geochemical alteration of wellbore cement in a generic geological CO_2 confinement site: tackling a difficult reactive transport modeling challenge, Journal of Hydrology, accepted under revision (2011).

[19] A. Fabbri, J. Corvisier, A. Schubnel, F. Brunet, B. Goffé, G. Rimmele, V. Barlet-Gouédard, Effect of carbonation on the hydro-mechanical properties of Portland cements, Cement and Concrete Research 39 (2009) 1156–1163.

[20] J. Taron, D. Elsworth, K.-B. Min, Numerical simulation of thermal–hydrologic–mechanical–chemical processes in deformable, fractured porous media, International Journal of Rock Mechanics and Mining Sciences 46 (2009) 842–854.

[21] C. Kervevan, S. Lanini, P. Audigane, Etude comparative des algorithmes de couplage des codes chimie-transport utilisés au BRGM, Premiers résultats à partir d'expérimentations numériques simples, Public Report BRGM-54904-FR, 2007.

[22] O. Coussy, Deformation and stress from in-pore drying-induced crystallization of salt, Journal of the Mechanics and Physics of Solids 54 (2006) 1517–1547.

[23] O. Coussy, Revisiting the constitutive equations of unsaturated porous solids using a Lagrangian saturation concept, International Journal for Numerical and Analytical Methods in Geomechanics 31 (2007) 1675–1694.

[24] O.S. Pokrovsky, Precipitation of calcium and magnesium carbonates from homogeneous supersatured solutions, Journal of Crystal Growth 186 (1998), 233–239.

[25] M. Brun, A. Lallemand, J. Quinson, C. Eyraud, A new method for the simultaneous determination of the size and the shape of pores: the thermoporometry, Thermochimica Acta 21 (1977) 59–88.

[26] M. Castellote, C. Andrade, X. Turrillas, J. Campo, G.J. Cuello. Accelerated carbonation of cement pastes *in situ* monitored by neutron diffraction, Cement and Concrete Research 38 (2008), 1365–1373.

[27] F. Lehner, Y. Leroy, Chapter 3: sandstone compaction by intergranular pressure solution, in: Y. Guéguin, M. Boutéca (Eds.), Mechanics of Fluid-Saturated Rocks, 2004.

[28] O. Coussy, Poromechanics, John Wiley & Sons, Ltd, 2004.

[29] T. Fen-Chong, E. Hervé, A. Zaoui. Micromechanical modelling of intracellular pressure-induced viscoelastic shrinkage of foams: application to expanded polystyrene. European Journal of Mechanics A/Solids 18 (1999), 201–218.

[30] T. Fen-Chong. Analyse Micromécanique des variations dimensionnelles de matériaux alvéolaires, PhD Thesis, Ecole Polytechnique, France, 1998.

[31] X. Château, L. Dormieux, Micromechanics of saturated and unsaturated porous media, International Journal for numerical and Analytical Method in Geomechanics 26 (2002) 831–844.

[32] R. Eymard, T. Gallouët, R. Herbin, The Finite Volume Method, in: Ph. Ciarlet, J.L. Lions (Eds.), Handbook of Numerical Analysis, Elsevier, 2000, pp. 715–1022.

[33] J. Corvisier, F. Brunet, A. Fabbri, S. Bernard, N. Findling, G. Rimmelé, V. Barlet-Gouédard, O. Beyssac, B. Goffé, Raman mapping and numerical simulation of calcium carbonates distribution in experimentally carbonated Portland cement cores, European Journal of Mineralogy 22 (2010) 66–74.

[34] T. Xu, E.L. Sonnenthal, N. Spycher, K. Pruess, "TOUGHREACT User's Guide", Lawrence Berkeley National Laboratory Report LBNL-55460, Berkeley, California, 2004.

[35] N. Neuville, E. Lécolier, G. Aouad, A. Rivereau, D. Damidot, Effect of curing conditions on oilwell cement paste behavior during leaching: experimental and modelling approaches, Comptes Rendus Chimie 12 (2009) 511–520.

[36] S. Ghabezloo, J. Sulem, J. Saint-Marc, Evaluation of a permeability–porosity relationship in a low-permeability creeping material using a single transient test, International Journal of Rock Mechanics & Mining Sciences 46 (2009) 761–768.

[37] E. Lécolier, A. Rivereau, G. Le Saoût, A. Audibert-Hayet, Durability of hardened Portland cement paste used for oilwell cementing, Oil & Gas Science and Technology 62 (2007) 335–345.

[38] M. Castellone, C. Andrate, Modelling the carbonation of cementitious matrixes by means of the unreacted-core model, UR-CORE, Cement and Concrete Research 38 (2008) 1374–1384.

[39] R.C. Weast, CRC Handbook of Chemistry and Physics, 58th edition, CRC Press, 1978.

[40] A. Pavese, M. Catti, S.C. Parker, A. Wall, Modelling of the thermal dependence of structural and elastic properties of calcite, $CaCO_3$, Physics and Chemistry of Minerals 23 (1996) 89–93.

[41] S. Ghabezloo, J. Sulem, S. Guédon, F. Martineau, J. Saint-Marc, Poromechanical behaviour of hardened cement paste under isotropic loading, Cement and Concrete Research 38 (2008) 1424–1437.

[42] S. Ghabezloo, Comportement thermo-poro-mécanique d'un ciment pétrolier, PhD thesis, Université Paris-est, Ecole des Ponts ParisTech, 2008, 194p.

[43] H.F.W. Taylor, Cement Chemistry, 2nd Ed. Thomas Telford Ltd., London, 1997.

[44] R.A. Cook, K.C. Hover, Mercury porosimetry of hardened cement pastes, Cement and Concrete Research 29 (1999) 933–943.

[45] A. Fabbri, Physico-mécanique des matériaux cimentaires soumis au gel-dégel, Edilivre-Aparis, 2008.

[46] Ph. Blanc, A. Lassin, P. Piantone (2008) THERMODDEM: a thermo-geochemical database for waste materials., in Waste-Eng - 2nd international conference on engineering for waste valorisation - Patras - Greece - 3-5/06/2008. http://thermoddem.brgm.fr/.

[47] M. Fleury, H. Deschamps, Electrical conductivity and viscosity of aqueous NaCl solutions with dissolved CO_2, Journal of Chemical Engineering Data 53 (2008) 2505–2509.